Applied Catalysis B: Environmental 277 (2020) 119193

Contents lists available at ScienceDirect

Applied Catalysis B: Environmental

journal homepage: www.elsevier.com/locate/apcatb

Importance of controllable Al sites in CHA framework by crystallization pathways for NH_3-SCR reaction

Juan Zhang[a], Yulong Shan[b], Ling Zhang[a], Jinpeng Du[b], Hong He[b], Shichao Han[a], Chi Lei[a], Sen Wang[c], Weibin Fan[c], Zhaochi Feng[d], Xiaolong Liu[e,*], Xiangju Meng[a,*], Feng-Shou Xiao[a,*]

[a] Key Lab of Applied Chemistry of Zhejiang Province, Department of Chemistry, Zhejiang University, Hangzhou, 310007, China
[b] State Key Joint Laboratory of Environment Simulation and Pollution Control, Research Center for Eco-Environmental Sciences, Chinese Academy of Sciences, Beijing, 100085, China
[c] State Key Laboratory of Coal Conversion, Institute of Coal Chemistry, Chinese Academy of Sciences, Taiyuan, 030001, China
[d] State Key Laboratory of Catalysis, Dalian Institute of Chemical Physics, Chinese Academy of Sciences, Dalian, 116023, China
[e] School of Materials, Sun Yat-Sun University, Guangzhou, 510275, China

ARTICLE INFO

Keywords:
NH_3-SCR reaction
CHA zeolites
Al sites
Organic templates
Crystallization pathways

ABSTRACT

As a commerical catalyst of high silica CHA zeolite for NH_3-SCR reaction, controllable Al sites in CHA framework for improving catalytic performance are rarely reported. In this work, two organic templates ($TMAda^+$ and $DMCHA^+$) were employed to prepare aluminosilicate CHA zeolite with similar Si/Al ratios, donated as CHA-T and CHA-D. Detailed characterizations demonstrate that two completely distinguishable crystallization pathways can be identified as the preferential formation of smaller D6R units for CHA-D with $DMCHA^+$ and larger 8MRs for CHA-T with $TMAda^+$, resulting in spatially closer Al sites in CHA-D than CHA-T. As an interpretation, CHA-D with more paired Al atoms in 6MR generating more hydrothermally stable Cu^{2+}-2Z sites contributes to higher activity than CHA-T at 400 − 550 °C. These results suggest that the crystallization pathways directed by rational choice of organic templates might be responsible for the controllable Al sites in the framework, which is important for designing efficient NH_3-SCR catalysts.

1. Introduction

The most important features of zeolites are their ion-exchange properties and structural architectures: the ion-exchange properties originate from balancing negative charge induced by tetrahedral Al atoms in framework sites (T sites), and the structural architectures contain pores with dimensions, cavities, and channels with small (eight-membered rings, 8MRs), medium (10MRs), and large (> 12MRs) micropore sizes, which lead to wide applications in the chemical and petroleum industries as well as water softening [1]. In the aluminosilicate zeolites, the ion-exchange properties are strongly related to the tetrahedral Al sites in frameworks. The Al state in the framework, *e.g.* the Al sites, has been recognized as an important factor in activity and selectivity, because it profoundly affects the accessibility of molecules to active sites (metal or protons) and the spatial constraints of the reaction field in the pores [2–5].

SSZ-13 zeolite (CHA), as one of eight-membered-ring (8MR) zeolites, has been extensively used as a highly effective catalyst for selective catalytic reduction (SCR) of nitrogen oxides (NO_X) with NH_3 [6,7]. For properly Cu-exchanged SSZ-13 zeolites, it is widely accepted that there are two chemically distinct active sites created by Cu ion monomers for standard NH_3-SCR reaction [8,9]. In line with previous studies, the isolated Cu^{2+} ions balanced by two opposite Al atoms in one regular 6MR window (Cu^{2+}-2Z) turn to be the energetically favorable site, while some $[Cu(OH)]^+$ ions balanced by one single Al atom prefer to locate in *cha* cages near 8MR window ($[Cu(OH)]^+$-Z) [10–12]. Beale et al. have revealed that $[Cu(OH)]^+$ ions in the 8MRs are active with high reducibility at low temperatures, whilst the isolated Cu^{2+} ions in the 6MRs are more active and durable at higher temperatures [13]. This conclusion has also been highlighted by Song et al. that in Cu-exchanged CHA zeolites, the stable Cu^{2+}-2Z active centers exhibit highly selectivity and remarkable hydrothermal stability, while $[Cu(OH)]^+$-Z active centers would be more facile to be converted into CuOx clusters at elevated reaction temperatures or after hydrothermal aging treatment [14]. Thus, a direct relevance for structure-activity relationship in CHA zeolite can be established between NH_3-SCR catalytic performances and the arrangements of Al atoms in the CHA framework such as isolated or paired Al sites [15,16]. Consequently, the productivity for

* Corresponding authors.
E-mail addresses: liuxlong9@mail.sysu.edu.cn (X. Liu), mengxj@zju.edu.cn (X. Meng), fsxiao@zju.edu.cn (F.-S. Xiao).

https://doi.org/10.1016/j.apcatb.2020.119193
Received 28 February 2020; Received in revised form 1 May 2020; Accepted 30 May 2020
Available online 01 June 2020

NH_3-SCR reaction can be further improved through controlling Al sites in the host zeolite CHA.

Generally, the nature and location of Cu species are affected by multiple factors including the zeolite structure, the Si/Al ratio, the Cu loading, and the synthesis strategies [17]. For a specific zeolite with a given Si/Al ratio and Cu loading, the synthesis strategies have expected to become a practical means of regulating the nature and location of Cu ions that are largely dependent on the distribution of Al atoms in zeolite framework. Several synthetic control over Al sites in zeolites has been studied [18–24], and in some cases, specific electrostatic stabilization effects could be presumed to be decisive [,21–24]. The conclusion has been drawn by Pinar et al. that the Al distribution over the zeolitic T sites can be varied by various organic templates [25]. Yokoi et al. has investigated the Al location that is determined by the type of organic templates and Na^+ ions used in the synthesis of ZSM-5 zeolite [26]. Devos et al. recently has drawn a mechanistic proposal for creating high paired Al content during FAU-to-CHA interzeolite conversion synthesis [27]. However, despite the great endeavor on promoting the correlation between synthetic strategies and Al distribution in zeolite framework, the detailed explanation under molecular level how such synthetic strategies control the Al sites are not completely understood, and the clear crystallization pathways underwent in the synthesis gel are ought to be specifically depicted under molecular level.

Spectroscopic methods have been proved to be powerful techniques and utilized in determining the intermediate structures upon crystallization [28,29]. Due to their advantageous characteristics in studying local intermolecular interactions, 2D ^{1}H DQ-SQ MAS NMR techniques have been successfully employed to investigate the spatial interaction between the template cations and the $SiO^-\cdots HO{-}Si$ hydrogen bonds in the framework [30]. The sound sensitivity in the T−OT− (T = tetrahedral site) bending region enables UV Raman spectroscopy to be conductive for detecting the disordered medium-range structure transformation of intermediates such as rings and large secondary building units (SBUs) [31].

Therefore, the relationship among synthesis-structure-activity could be investigated by employing CHA zeolites as a suitable model. Here, two kinds of organic templates including N, N, N-trimethyl-1-adamantanammonium ($TMAda^+$) cations and N, N-dimethylcyclohexylammonium ($DMCHA^+$) cations have been used to prepare high silica CHA zeolites, of which exhibit different catalytic performance in standard NH_3-SCR reactions. To account for it, the combination of 2D NMR and UV Raman techniques is employed to provide the molecular level information about the roles of two organic templates played in the formation of CHA and their corresponding crystallization pathways from discrete building units. The resulting proximate Al arrangements have been practically probed through DR UV–vis spectroscopy using Co^{2+} titration method. It is the difference in the crystallization pathways that leads to the varying Al sites in the CHA framework by adjusting the organic template cations, which obviously influences the catalytic activity for NH_3-SCR reaction. The uncovered synthesis-structure relations should be encouraging and might offer an opportunity to design new highly efficient catalysts in the future.

2. Experimental

2.1. Materials

The chemicals used in this work included sodium hydroxide (NaOH, AR, 96 %, Sinopharm Chemical Reagent Co., Ltd.), sodium meta-aluminate ($NaAlO_2$, AR, Sinopharm Chemical Reagent Co., Ltd.), colloidal silica (40 wt.% SiO_2 in water, Sigma-Aldrich Co., Ltd.), N, N, N-trimethyl-1-adamantanammonium hydroxide solution (TMAdaOH, 25 wt. %, Sichuan Zhongbang Co., Ltd.), sodium metasilicate nonahydrate ($Na_2SiO_3{\cdot}9H_2O$, AR, SiO_2 of 20 wt.%, Aladdin Chemistry Co., Ltd.), aluminum sulfate ($Al_2(SO_4)_3{\cdot}18H_2O$, AR, 99 %, Sinopharm Chemical Reagent Co., Ltd.), solid silica gel (SiO_2, Qingdao Haiyang Chemical Reagent Co, Ltd.), N, N-dimethylcyclohexylamine (AR, 98 %, Aladdin Chemistry Co., Ltd.), bromoethane (AR, 98 %, Aladdin Chemistry Co., Ltd.), anhydrous diethyl ether (AR, 99.5 %, Aladdin Chemistry Co., Ltd.), ethanol (AR, 99.7 %, Shanghai Lingfeng Chemical Reagent Co., Ltd.), deionized water (homemade), ammonium nitrate (NH_4Cl, AR, 99 %, Beijing Chemical Reagent Co., Ltd.), sodium chloride (NaCl, AR, 99.5 %, Sinopharm Chemical Reagent Co., Ltd.), cobalt nitrate hexahydrate ($Co(NO_3)_2{\cdot}6H_2O$, AR, 98.5 %, Sinopharm Chemcal Reagent Co., Ltd.), and copper nitrate ($Cu(NO_3)_2$, AR, Sinopharm Chemcal Reagent Co., Ltd.). All synthesis reagents were used without further purification.

2.2. Zeolite syntheses

The CHA-T zeolite was synthesized hydrothermally by using TMAdaOH as organic template. As a typical run, a certain amount of TMAdaOH, NaOH, $NaAlO_2$, and deionized water were mixed, followed by addition of Ludox-40 under vigorous stirring. After stirring for 2 h, the starting gel with molar composition of 1.0 SiO_2: 0.032 Al_2O_3: 0.18 Na_2O: 22 H_2O: 0.12 TMAdaOH was obtained and transferred into a Teflon-lined autoclave, heating in oven at 160 °C for different crystallization time. The product was finally obtained after washing with deionized water and drying at 100 °C for 1 h, which was denoted as CHA-T, where T stands for $TMAda^+$ cations.

The CHA-D zeolite was synthesized from solvent-free route using DMCHABr as organic template. After grinding the raw materials, the starting gel with molar composition of 1.0 SiO_2: 0.035 Al_2O_3: 0.18 Na_2O: 0.12 DMCHABr was obtained and transferred into a Teflon-lined autoclave, heating in oven at 180 °C for different crystallization time. The product was finally obtained after washing with deionized water and drying at 100 °C for 1 h, which was denoted as CHA-D, where D stands for $DMCHA^+$ cations.

2.3. Ion exchange methods

The fully crystallized CHA-T and CHA-D samples were calcined at 550 °C for 5 h to remove the organic templates. The H-form samples (H-CHA-T and H-CHA-D) were ion-exchanged with 1 M NH_4Cl solution at 80 °C twice, followed by calcination at 550 °C for 5 h. For NH_3-SCR reactions, the Cu-form samples (Cu-CHA-T and Cu-CHA-D) were obtained by further ion-exchanging the H-form samples with 1 M $Cu(NO_3)_2$ aqueous solution at 80 °C twice, followed by calcination at 550 °C for 5 h. For investigating the Al sites in the framework, the Co-form samples (Co-CHA-T and Co-CHA-D) were prepared by reversely ion-exchanging the H-form samples with 1 M NaCl solution at 80 °C for 6 h three times, followed by repeated treatment of the samples with 0.05 M $Co(NO_3)_2{\cdot}6H_2O$ solution at 80 °C for 12 h three times under stirring conditions, in order to guarantee that the maximum ion exchange of Co^{2+} ions can be achieved [32].

2.4. Catalytic tests

The acidity of the catalysts was measured by the temperature-programmed-desorption of ammonia (NH_3-TPD) using a Micromeritics ChemiSorb 2720 Pulse Chemisorption System with the procedures as follows: the fresh H-CHA-T, H-CHA-D, Cu-CHA-T, and Cu-CHA-D samples (0.1 g, 40–60 mesh) were pretreated at 550 °C in a He flow for 60 min, followed by the adsorption of NH_3 in NH_3-He (10 vol% NH_3) gas mixture at 100 °C for 30 min. After saturation, the catalyst was purged by He flow for 30 min to remove the physically adsorbed ammonia on the sample. Then, desorption of NH_3 was carried out from 100 to 750 °C with a heating rate of 10 °C/min.

The types of copper species was measured by the temperature-programmed-reduction of hydrogen (H_2-TPR) using a Micromeritics ChemiSorb 2720 Pulse Chemisorption System with the procedures as follows: the fresh and hydrothermally aged Cu-CHA-T, and Cu-CHA-D

samples (0.1 g, 40–60 mesh) were heated from 50 °C to 750 °C with a heating rate of 10 °C/min under a 5 % H_2/Ar flow in a rate of 50 ml/min. The thermal conductivity detector (TCD) was used to detect the consumption of hydrogen by the samples.

The standard NH_3-SCR reactions over fresh and hydrothermally aged (HTA) at 750 °C for 16 h Cu-CHA-T and Cu-CHA-D (donated as Cu-CHA-T-fresh, Cu-CHA-D-fresh, Cu-CHA-T-HTA 750 and Cu-CHA-D-HTA 750, respectively) samples were carried out in a fixed-bed quartz reactor with a gaseous mixture containing 500 ppm of NO, 500 ppm of NH_3, 10 % of O_2, 10 % of H_2O and N_2 as a balance gas. The gas hourly space velocity (GHSV) was 80,000 h^{-1}. NH_3 oxidation reactions were conducted under identical conditions except that the NO feed was stopped.

2.5. Characterization

The crystalline structure of the samples was determined by Powder X-ray diffraction (XRD) patterns (Rigaku Ultimate VI X-ray diffractometer) using Cu Kα (λ = 1.5406 Å) radiation at 40 kV and 40 mA. The argon sorption isotherms at the temperature of liquid nitrogen were measured using Micromeritics ASAP 2020 M and Tristar system. Thermogravimetric curves (TG) were performed on an SDT Q600 Simultaneous DSC-TGA in flowing air with heating rate of 10 °C/min. Scanning electron microscopy (SEM) experiments were performed on Hitachi SU-1510 and SU-8010 electron microscopes. The sample composition was determined by inductively coupled plasma (ICP) with a Perkin-Elmer 3300DV emission spectrometer. The electron paramagnetic resonance (EPR) spectra experiment were conducted on a Bruker A300 EPR Spectrometer of the hydrated fresh and hydrothermally aged at 750 °C CHA-T and CHA-D samples. Powder samples (~100 mg) were contained in 4 mm OD quartz tubes and spectra were recorded at 120 K temperatures to “freeze” Cu(II) ions. Microwave power was 20.31 MW, and the frequency was 9.408 GHz. The field was swept by 1200 G in 48 s and modulated at 100 kHz with 1 G amplitude. A time constant of 81.92 ms was used. The relative quantification of isolated Cu^{2+} ions in fresh and HTA Cu-CHA-D and Cu-CHA-T samples were referenced to $CuCl_2$ dispersed in silicon powder with the Cu^{2+} content about 2.5 %.

UV Raman spectra were recorded with a Jobin–Yvon T64000 triple-stage spectrograph with spectral resolution of 2 cm^{-1} and UV laser line at 266 nm. All the obtained UV Raman spectra were collected on the solid products filtered after quenched at different given crystallization time with measuring time of 300 seconds and one-time accumulation. FT-IR spectra were recorded on Thermo Scientific Nicolet iS5 FT-IR spectrometer. Solid-state ^{29}Si and ^{27}Al MAS NMR experiments were performed on a Bruker AVANCE-III 500 spectrometer. ^{1}H MAS NMR and 2D ^{1}H DQ-SQ MAS NMR spectra were carried out on a Bruker AVANCE-III 500 spectrometer using a 1.9 mm triple resonance MAS probe at a spinning frequency of 40 kHz, typical π/2-pulse lengths of 1.5 μs, and a recycle delay of 2 s. The spectra were referenced with respect to tetramethylsilane (TMS) using solid tetrakis(trimethylsilyl) silane as a secondary standard (0.27 ppm for ^{1}H). The diffuse reflectance ultraviolet-visible (DR UV–vis) spectra were recorded on an Agilent Cary 5000 UV–vis-NIR spectrophotometer equipped with a poly (tetrafluoroethylene) integrating sphere.

2.6. Computational methods

The computation method used in this study was described as follows: the 15 T 8MR (Fig. S7) cluster structure was extracted from the CHA (SSZ-13) crystallographic structural data (http://www.iza-structure.org/databases/). The terminal oxygen (O) atoms are saturated with hy-drogen (H) atoms that were positioned on the vector from the O atom to the Si atom. The geometry optimizations were carried out at the level of B3LYP/6-311g (d, p), and Van der Waals correction was included by using Grimme’s D3 method. During the structure optimizations, the dangling H atoms of 8MR cluster were fixed to preserve the integrity of ring structure, while all other framework atoms were relaxed to their equilibrium position including the adjacent TMAdaOH molecule. Based on the optimized structures of 8MR together with TMAdaOH, the Raman vibrational frequency analysis was carried out simultaneously, as referred to the experiment Raman results. All the calculations were performed by using the Gaussian 09 package.

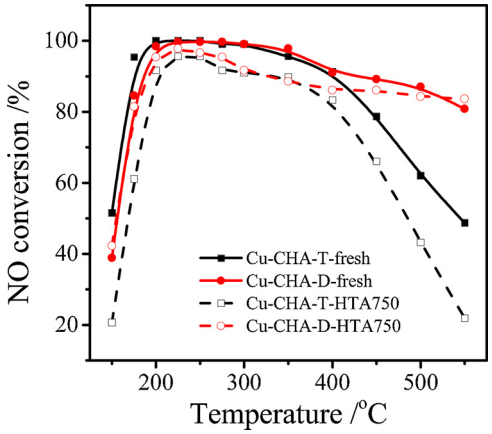

Fig. 1. Dependences of the NO conversion on temperature for the standard NH_3-SCR reactions over the fresh and 750 °C aged Cu-CHA-T and Cu-CHA-D catalysts.

3. Results and discussion

3.1. Evaluation of catalytic performance in standard NH_3-SCR reaction

Two synthetic routes were chosen for the preparation of high silica CHA zeolites using organic templates of $TMAda^+$ and $DMCHA^+$ cations, designated as CHA-T and CHA-D, respectively. Fig. S1 shows X-ray diffraction patterns of both samples for various stages in the crystallization, giving characteristic peaks at 9.5°, 16.1°, 20.7°, and 25.0°, which are associated with well crystallized SSZ-13 zeolite [33].

Fig. 1 displays the catalytic performances for standard NH_3-SCR reactions over the fresh and aged (hydrothermally aging at 750 °C, donated as HTA750) CHA-T and CHA-D catalysts. For the fresh Cu-exchange CHA catalysts, Cu-CHA-T catalyst shows a slightly higher activity in the NO conversion than Cu-CHA-D below ~250 °C. However, after the reaction temperature increased in the range of 400 ~ 550 °C, a noticeable decrease has taken place over the fresh Cu-CHA-T catalyst of which the activity dropped down to 50 %, compared with the fresh Cu-CHA-D catalyst that still kept the NO conversion above 80 %. In particular, the two catalysts exhibit more remarkable distinction in the activity of NO conversion after hydrothermal aging treatment at 750 °C, in which the aged Cu-CHA-D catalyst have shown more excellent catalytic performance than the aged Cu-CHA-T catalyst both in low and high reaction temperature. Moreover, NH_3 oxidation reactions are further explored and shown in Fig. S2. The catalytic activity for NH_3 oxidation reactions over fresh Cu-CHA-D catalyst is always lower than fresh Cu-CHA-T catalyst, and an apparent enhancement of NH_3 conversion over both hydrothermally aged catalysts are also observed, indicating that fresh Cu-CHA-T shows stronger NH_3 oxidation ability than fresh Cu-CHA-D, and the hydrothermal aging treatment will result in the increase of NH_3 oxidation activity. Therefore, the fresh Cu-CHA-T seems more supportive to active NH_3 molecules and thereby promotes their selective catalytic reduction with NO that would be beneficial to enhance the NO conversion in low reaction temperature below ~250 °C. However, the weaker NH_3 oxidation ability of fresh Cu-CHA-D would effectively reduce the competing and undesired oxidation of NH_3 that contribute to the higher SCR activity in elevated reaction

temperature.

In order to figure out the drastic differences in catalytic activity of NH_3-SCR reaction, the chemical analyses are inquired into and presented in Table S1 and Fig. S3, which reveal that CHA-T and CHA-D samples possess a high degree of similarity in textural parameters including micropore volume and BET surface areas, Si/Al ratios, Cu loading and cubic morphology. In spite of similar chemical components, the evident distinction in NH_3-TPD profiles (Fig. S4) suggests different acidic sites and strength over fresh H/Cu-CHA-T and H/Cu-CHA-D samples. H_2-TPR patterns in Fig. S5 over fresh and aged Cu-type CHA-T and CHA-D samples also recommend the existence of different nature and location of Cu ions in the framework. For the fresh Cu-CHA catalysts, the low and high temperature peaks around ~247 and 428 °C are assigned to reduction of $[Cu(OH)]^+$-Z sites and Cu^{2+}-Z sites [14], respectively. Obviously, more Cu^{2+}-Z sites could be observed in Cu-CHA-D with contrary to more $[Cu(OH)]^+$-Z sites in Cu-CHA-T. For the aged Cu-CHA-T catalysts, the peak around 300 °C can be assigned to the reduction of CuOx species. A larger proportion of CuOx cluster accumulation can be observed in Cu-CHA-T than Cu-CHA-D during hydrothermal aging treatment. To quantify the relative amounts of active Cu^{2+} ions, EPR spectra are collected at 120 K and displayed in Fig. S6 over fully hydrated fresh and aged Cu-type CHA-T and CHA-D samples, where all existing isolated Cu-ions (including $[Cu(OH)]^+$ and Cu^{2+}) are EPR active, while CuOx clusters are EPR silent. The decreased EPR signal of hydrothermally aged samples are observed compared with that of fresh samples. In addition, the relatively amounts of isolated Cu^{2+} ions are further calculated by double integrating the EPR signals in Fig. S7. After hydrothermal aging at 750 °C, an obvious reduction of the amounts of isolated Cu^{2+} ions occurs, especially for Cu-CHA-T samples, indicating that much greater amounts of active isolated Cu^{2+} ions in Cu-CHA-T converted into CuOx clusters than in Cu-CHA-D that contains more Cu^{2+}-Z sites, which is in good agreement with previous reports by Shan et al. that the stable Cu^{2+}-2Z species coordinated with paired Al sites are proved to effectively inhibit the accumulation of CuOx clusters during hydrothermal aging [16,34].

Combined with above results, it is reasonable to conclude that although CHA-T and CHA-D samples share similar chemical properties, there are plenty of dissimilarities in the catalyst acidity and the nature of Cu ions between these two samples that lead to different catalytic performances, both of which should be directly determined by various Al sites [12,35–37]. Therefore, what can be inferred is that catalytic performances can be influenced by the rational choice of organic templates in the synthesis that are responsible for local Al siting, overall framework structure. Above intriguing observations raise two elemental issues: What role does the organic template play in the zeolite crystallization, and how does it affect the arrangement of Al sites in the framework? Integrated techniques like 2D ^{1}H DQ-SQ NMR, UV Raman, and DR UV–vis spectroscopy were employed to systematically interpret these two questions.

3.2. Roles of organic templates played in CHA zeolite synthesis

Solid state NMR techniques have highlighted the significance of weak and noncovalent intermolecular forces in pre-nucleation phases during zeolite formation [38]. To explore the role of organic templates played in the crystallization of CHA zeolites, 2D ^{1}H DQ-SQ NMR experiments have been carried out for characterizing the conformation changes of two organic templates occluded in CHA structures, and probe the spatial correlationship between organic template molecules and the negative charges in the framework, where the chemical shift of a correlation peak in the DQ dimension is the sum of the isotropic chemical shifts of the two same or different spins in the SQ dimension.

2D ^{1}H DQ-SQ NMR spectra of CHA-T samples are displayed in Fig. 2. Through analyzing the location and correlationship of off-diagonal and diagonal signals in the spectra, the signal at 3.38 ppm can be assigned to the methyl groups adjacent to the nitrogen of $TMAda^+$ cations. Before heating treatment (0 h) and after 12 h heating, there are no off-diagonal cross- correlation signals in Fig. 2a and b, indicating that the methyl group of $(CH_3)_3N$- is away from the methylene groups in adamantyl. However, the appearances of the off-diagonal cross-correlation signals at (2.42, 2.42 + 3.38) and (3.38, 3.38 + 2.32) in Fig. 2c and d suggests that the methyl group of $(CH_3)_3N$- is close to the methylene groups in adamantyl after the formation of highly-crystallized SSZ -13 zeolite.

All signals from adamantyl group in $TMAda^+$ cation is also assigned and shown in Fig. S8. It is well accepted that there are two conformational isomers for $TMAda^+$ molecule. Obviously, the conformer of $TMAda^+$ in the early stage (A) (the signal at 2.02 ppm in Fig. 2a and b) is more thermally dynamic stable than that in crystallized SSZ-13 framework (B) (the signals at 2.32 ppm in Fig. 2c and d). Compared with XRD patterns on the onset of Bragg peak appearance, the changes in conformer reflect that the conformational changes coincided with the formation of a prephase or microcrystallites that appear to be a necessary step to enable the CHA framework to form. In addition, a characteristic ^{1}H NMR chemical shift near 10 ppm can be observed in all ^{1}H NMR spectra of CHA-T samples with different heating time of 0, 12, 36 and 72 h, as displayed in Fig. S9, evidencing the existing defective $SiO^-\cdots HO{-}Si$ hydrogen bonds in CHA-T zeolite framework [30].

To further detect the spatial interactions between the organic template cations and the $SiO^-\cdots HO{-}Si$ hydrogen bonds in the framework during crystallization, the enlarged spectra of Fig. 2c is illustrated in Fig. S10 and all correlated signals from $TMAda^+$ cations are circled. The off-diagonal cross-correlation signals at (10.00, 10.00 + 3.38) and (10.00, 10.00 + 2.72) show that the existing defective $SiO^-\cdots HO{-}Si$ hydrogen bonds within the framework are spatially close to the methyl groups and the methylene groups in adamentyl of $TMAda^+$ cations, which indicates strong electrostatic interactions between the cationic $TMAda^+$ and the defect sites in large membered ring (*e.g.* 8MRs) of CHA framework, and the 8MR window might be around the neck of $TMAda^+$ molecule.

Studying the conformation of organic molecules within the frameworks could understand the organic-inorganic interactions and structure direction roles of organic molecules. Above results imply that the major driving force for the conformational changes of $TMAda^+$ cations is to fit $TMAda^+$ molecule in the zeolite cavities for minimizing unoccupied free space to maximize the interaction with negative charges in the framework, just in good agreement with the previous reports about the structure-directing effects and occurrence of conformational changes of organic template (TEA^+) conformers in the formation of aluminophosphate zeo-type materials [39] and aluminosilicate zeolites [40].

Fig. 3 shows 2D ^{1}H DQ-SQ NMR spectra of CHA-D samples about the off-diagonal and diagonal cross-correlation signals among the protons in $DMCHA^+$ cations. By analyzing the location and correlationship of off-diagonal and diagonal signals in the spectra, the signal at 1.64 ppm or 2.24 ppm is assigned to the methyl groups and the methylene groups of ethyl adjacent to the nitrogen of $DMCHA^+$ cations, and the signal at 3.18 or 3.14 ppm is assigned to the methylene groups of cyclohexyl adjacent to the nitrogen of $DMCHA^+$ cations.

All other signal assignments from cyclohexyl groups are shown in Fig. S11. The signal assignments are as follows: (i) before heating treatment (0 h) and after12 h heating, the tertiary ammonium group of $DMCHA^+$ is mainly at an *e* (equatorial) bond on the cyclohexene (A, the signals at 1.64 and 3.18 ppm in Fig. 3a and b), because this conformation is more thermodynamically stable; (ii) when the SSZ-13 crystallites formed, the *a* (axial) bond conformation (B) of $DMCHA^+$ is dominant and kinetically stable(the signals at 2.24 and 3.14 ppm Fig. 3c and d), which tends to be more advantageous for the construction of small membered ring (*e.g.* 6MRs and D6R units) with the support of more favorable quaternary ammonium head conformer, indicating that $DMCHA^+$ cations were occluded in the CHA zeolite cages

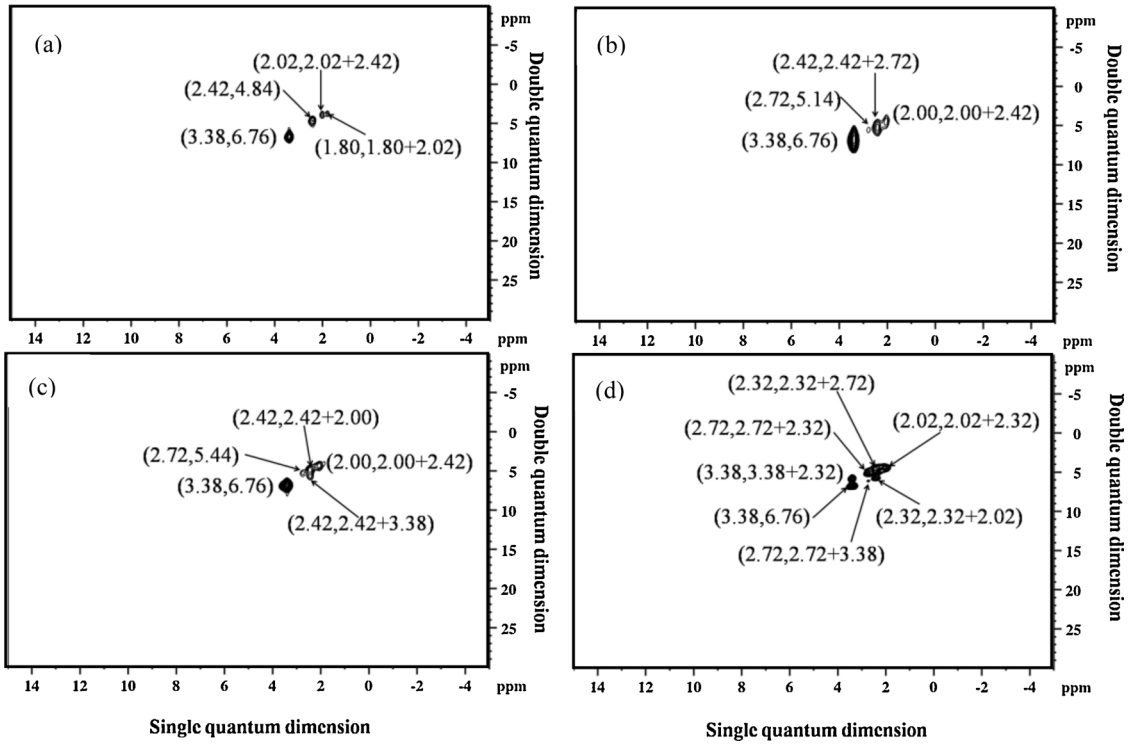

Fig. 2. 2D ^{1}H DQ-SQ NMR spectra of CHA-T with TMAda^{+} cations as organic template for different periods of time (a: 0 h; b: 12 h; c: 36 h; d: 72 h).

as an isolated cation geometrically fitted within the zeolite cavities to minimize unoccupied free space. 2D ^{1}H DQ-SQ MAS NMR spectra in Fig. 3 do not detect the spatial correlation between the DMCHA^{+} cations and the SiO^{-}···HO—Si hydrogen bonds in the framework during the crystallization. No chemical shift near 10 ppm could be traced in ^{1}H NMR spectra of CHA-D samples as shown in Fig. S12 with different heating time of 0, 12, 36 and 72 h also indicate the absence of defective SiO^{-}···HO—Si hydrogen bonds in CHA-D framework. These results suggest that the positive charges from DMCHA^{+} cation should be balanced by the negative charges provided by Si-O-Al structural units

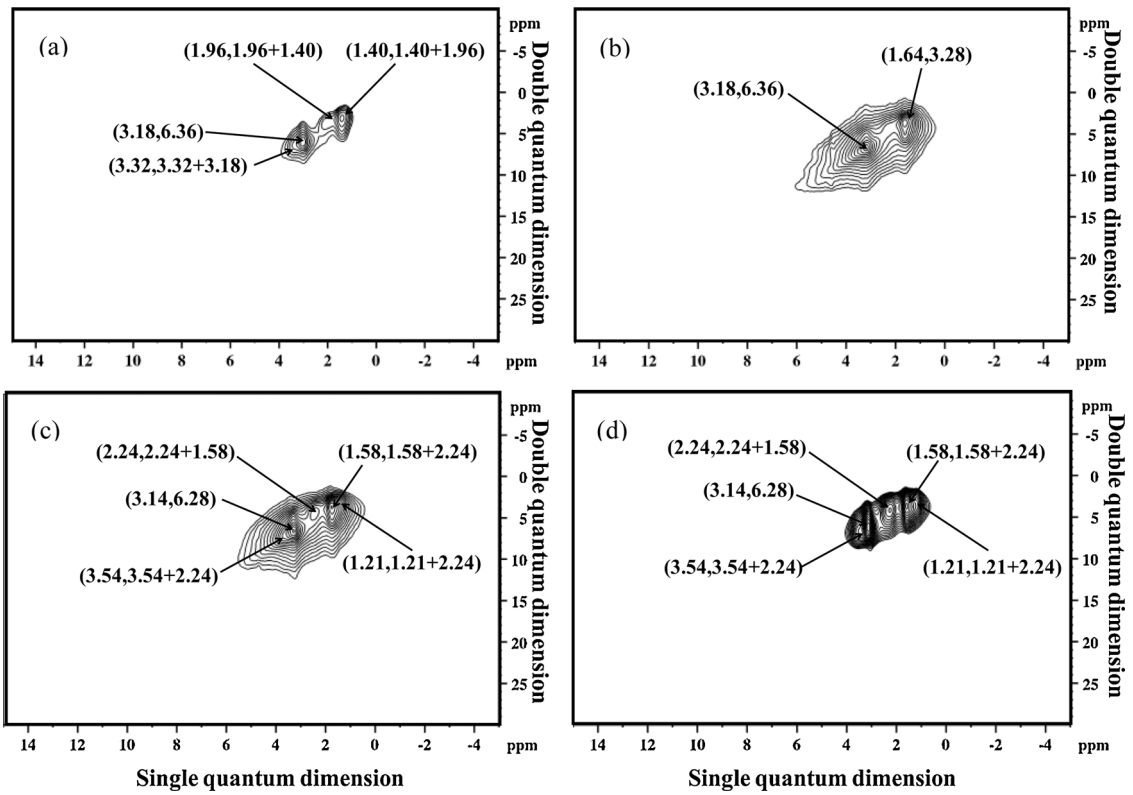

Fig. 3. 2D ^{1}H DQ-SQ NMR spectra of CHA-D with DMCHA^{+} cations as organic template for different periods of time (a: 0 h; b: 12 h; c: 36 h; d: 72 h).

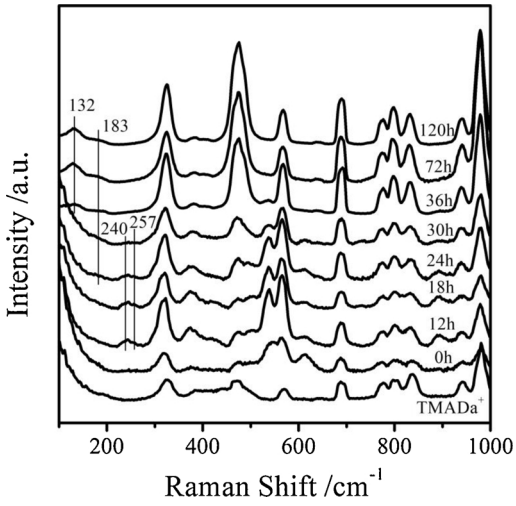

Fig. 4. UV Raman spectra recorded for the solid phase of zeolite CHA-T with $TMAda^+$ cations as organic template for different periods of heating time.

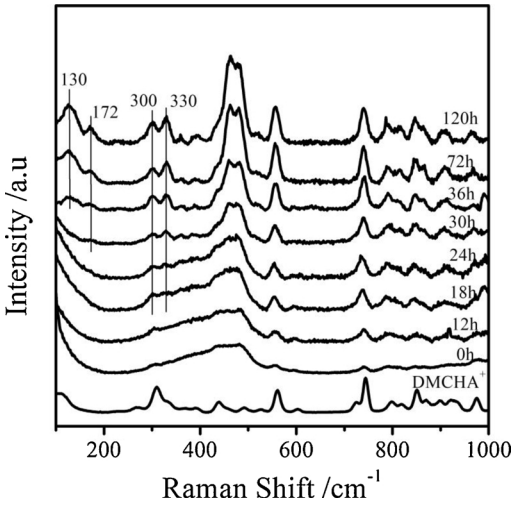

Fig. 5. UV Raman spectra recorded for the solid phase of zeolite CHA-D with $DMCHA^+$ cations as organic template for different periods of heating time.

during the growth of CHA-D crystals, and the small diameter of $DMCHA^+$ molecule is more advantageous in coordinately matching the structure of small units with Al substituted (*e.g.* 6MRs and D6R units).

What can be concluded and answered from the NMR results is that the roles of these used organic templates with preferable conformers fall into two different categories: $TMAda^+$ cations exhibiting a strong electrostatic interaction with the negative $SiO^-\cdots HO{-}Si$ hydrogen bonds in large membered ring in the framework, whilst $DMCHA^+$ cations showing a strong interaction with the negative Si-O-Al structure in smaller units by means of coordination effect. These two effects may bring about varying crystallization pathways in synthesizing the same CHA framework. To investigate the influence of organic templates on the crystallization pathways, UV Raman experiments have been carried out for detecting the possible active intermediates during crystallization.

3.3. Investigation of crystallization pathways effected by organic templates

UV Raman spectra recorded for the solid phase of CHA-T zeolites with $TMAda^+$ cations as organic template for different crystallization time, are shown in Fig. 4. After 12 h heating when the trace XRD characteristic peaks of CHA framework can be detected (enlarged illustration in Fig. S1a), two Raman bands at 240 and 257 cm^{-1} start to appear, and the assignment of the former band is normally correlated to the vibration frequencies of 8MRs in the solid phase [41]. For further verification, theoretical simulation has been performed based on the proposed intermediates displayed in Fig. S13 and Table S2. As a result, the former band at 240 cm^{-1} appears to be the vibrational frequency of 8MR structure by the aid of $TMAda^+$ cation, while the latter band at 257 cm^{-1} is associated with the vibration mode of $TMAda^+$ cation. 2D ^1H DQ-SQ NMR results have confirmed the strong electrostatic interactions between the $TMAda^+$ cations and the defective framework, which made it possible for the designated formation of 8MRs as a metastable structure in the solid phase during crystallization. When the heating time is up to 24 h, a weak band at 183 cm^{-1} begins to be observed that is possibly related to the bending modes of cha cage in the solid phase. After crystallized for 36 h, another new band appears at 132 cm^{-1}, which can only be found in the highly-crystallized SSZ-13 with ordered channels [31].

All other bands in the UV Raman spectra of the solid phases with various heating time in Fig. 4 are mainly from $TMAda^+$ cation. Above observations obviously manifest that the formation of 8MRs is much earlier than that of *cha* cage when $TMAda^+$ cation was used as organic template. In particular, the gradual decreasing intensities of band at 240 cm^{-1} is simultaneously accompanied by the increasing intensities of band at 183 cm^{-1}, indicating that the formation of *cha* cage is derived from the consumption of 8MRs, and afterwards the well-crystallized SSZ-13 structure will be formed. The FT-IR spectra also correlate with the UV Raman results as shown in Fig. S14a, in which the characteristic peak around 640 cm^{-1} typically assigned to D6R units in CHA framework [42,43] starts to appear only after heating for 36 h when the 8MRs and *cha* cage have been constituted, further validating the fact that the organic templates $TMAda^+$ cations will preferentially facilitate the formation of 8MRs prior to *cha* cage, and then D6R units can be arranged by coupling among the *cha* cage, in highly consistence with previous researches reported by Hong and co-workers [42].

Fig. 5 shows UV Raman spectra recorded for the solid phase of CHA-D zeolites with $DMCHA^+$ cations as organic template for different crystallization time. After 18 h heating when the trace XRD characteristic peaks of CHA-D framework can be detected (Fig. S1b), two Raman bands at 300 and 330 cm^{-1} start to appear, which can be assigned to the bending mode of D6R units in the solid phase [29,44], a perfect match with FT-IR spectra (Fig. S14b) that the vibrational frequency of D6R units around 640 cm^{-1} shows up at the same time [42,44]. When the heating time is up to 30 h, the weak band at 172 cm^{-1} comes out and corresponds to the bending modes of *cha* cage formed in the solid phase. After crystallized for 36 h, another new band appears at 130 cm^{-1} that can also only be found in the highly-crystallized SSZ-13 zeolite. All other bands in the UV Raman spectra of solid phases with various heating time in Fig. 5 are mainly from $DMCHA^+$ cation. These results indicate that the formation of D6R units is much earlier than that of *cha* cage when $DMCHA^+$ cation was used as organic template, where the D6R units seem to be more critical for the assembly of *cha* cage than 8MRs and afterwards the well-crystallized SSZ-13 structure, exactly as revealed by 2D ^1H DQ-SQ NMR results that the role of $DMCHA^+$ cations played in the crystallization of CHA-D is primarily to geometrically fitted within the zeolite cavities that support the construction of small ring structures with Al substituted (*e.g.* 6MRs and D6R units).

When using two different organic templates $TMAda^+$ and $DMCHA^+$ cations, there certainly exist two completely distinguishable crystallization pathways for synthesizing the same CHA structure. Besides, the coordination environments of Si and Al atom in CHA framework also respond to diverse evolution during crystallization as shown in the solid state ^{29}Si and ^{27}Al NMR spectrum (Figs. S15, S16 and Table 3). The NMR spectra showing a higher proportion of Q^3 and Q^4 units in CHA-D than CHA-T, as well as the remaining tetrahedral coordination environment of aluminum in CHA-D, indicate the high-silica nature and

quicker insertion of aluminum in CHA-D that contribute to a favorably stable circumstance for the assembly of more stable smaller units (6MR and D6R), compared with CHA-T that low-silica nature and slower release of aluminum suggest more defective structure in larger units (8MR). Therefore, what can be learned is that the formation of 8MRs is superior to the formation of *cha* cages during the crystallization of SSZ-13 with $TMAda^+$ cation, while the formation of D6R units is superior to the formation of *cha* cages instead of 8MRs during the crystallization of SSZ-13 with $DMCHA^+$ cation. Such great differences in crystallization pathways will significantly influence the nature and location of Al atoms, *e.g.* isolated Al sites or close Al sites.

3.4. Characterization of nature and distribution of Al sites

According to the observations from 2D ^1H DQ-SQ NMR and UV Raman spectra, the formation of 8MRs is superior than that of *cha* cages when $TMAda^+$ cation was used (Fig. 4), owing to the specific spatial correlation between the cationic $TMAda^+$ and the $SiO^-\cdots HO{-}Si$ hydrogen bonds in 8MRs of the framework (Fig. 2). Both $SiO^-\cdots HO{-}Si$ hydrogen bonds and Al substitution in the zeolite framework act as the negative charge centers to balance the positive charges from organic template cations. Such strong electrostatic interactions between the positive charges from $TMAda^+$ and the negative charges from Al substituted 8MRs are apt to control the Al atoms mainly located in 8MRs window. Consequently, the regulated Al atoms in the 8MRs (3.8 × 3.8 Å) of CHA-T zeolite are relatively far apart from each other compared with in smaller 6MRs, indicating the limitation of the close Al sites but abundant amounts of isolated Al sites in this type of zeolites.

Since the reorganization of aluminosilicate species was accompanied by the conformational rearrangement of $DMCHA^+$ to yield the well-crystallized CHA-type zeolite (Fig. 3), it can be learned that both the location and conformation of the organic templates are critical for the formation of zeolites structure. As UV Raman spectra reflect that D6R units are formed earlier than *cha* cages during the crystallization with $DMCHA^+$ cations (Fig. 5), it is evidenced that the negative charges from Al substitution are mainly located in the D6R units or regular 6MRs. Because of shorter diameter of 6MR than 8MR in the opening, the Al atoms would be closer to each other in CHA-D than CHA-T samples, resulting in the ample close Al sites in the CHA-D. The relevance of these results relies on the fact that the Al sites can be varied by adjusting the templating molecules.

For the purpose of further verifying the different distributions of Al sites in CHA-T and CHA-D zeolites, ion-exchange of Co(II) as probing cations was monitored by DR UV–vis spectroscopy [20,27,45,46] and inductively coupled plasma (ICP) tests. Table 1 displays the ICP analysis from two Co-exchanged CHA samples that the proportion of Al_{close} and $Al_{isolated}$ values are about 47.7 % and 52.3 % for CHA-T, as well as 83.6 % and 16.4 % for CHA-D, respectively, in good accordance with the NMR data and UV Raman that illustrate the preferential formation of 8MRs in CHA-T and D6R units in CHA-D, leading to the spatially closer Al sites in CHA-D than CHA-T and a majority of isolated Al atoms populated in CHA-T. More specifically, the Al_{close} involves in two types of Al siting Al_{paired} and $Al_{unpaird}$, wherein the corresponding cationic sites of bare divalent Co cations can be created by the Al_{paired} sites.

Three cationic sites formed by the siting of Al_{paired} for divalent cations were distinguished for CHA zeolites, denoted as σ-, τ- (including τ^{2Si} and τ^{3Si}), and ω-types, where the σ sites represent the two opposite Al atoms seated in the regular 6MRs, the τ sites seated in the 8MRs, and the ω sites seated in the D6R units with each Al atom in a different 6MR [32,46–48]. Seven Gaussian curves were employed in the decomposition Co^{2+} spectra for satisfying the description of spectroscopic predominating components σ, τ, or ω sites are shown in Fig. S17, and the assignment of each curves were clarified based on the recent publication by Mlekodaj et al. [46]. In addition, their assignments and percentage of each absorption bands in the individual sites of CHA-T and CHA-D were listed in the Tables S4 and 1 . As a result, the concentration of Al_{paired} seated in the regular 6MRs, 8MRs, and D6R units are 1.5 %, 58.1 % and 40.4 % for CHA-T samples, as well as 14.4 %, 38.1 % and 47.1 % for CHA-D samples, respectively, indicating that the siting of Al_{paired} balancing bare Cu^{2+} ions spread over 8MRs in CHA-T and D6R units in CHA-D.

In particular, it is noteworthy that σ sites formed by Al_{paired} sites with an Al-O-$(Si\text{-}O)_2$-Al sequence in the regular 6MRs are much more abundant of CHA-D samples (14.4 %) than CHA-T samples (1.5 %), which were rendered to be the most energetically stable cationic sites for accessible divalent cations in CHA zeolites (Cu^{2+}, Co^{2+} and Fe^{2+}) [11,46,49]. The higher proportion of Al_{paired} sites in 6MRs of CHA-D would be more conductive to the formation of more comparable amount of isolated Cu^{2+} ions located in 6MRs, widely recognized as Cu^{2+}-2Z species, in contrast to CHA-T containing slightly more $[Cu(OH)]^+$-Z species because of the primarily isolated Al sites, supported by the NH_3-TPD, H_2-TPR, and EPR results (Figs. S4–6). As described above, Cu^{2+}-2Z species is thermodynamically favorable for NH_3-SCR reactions with higher durability in the high temperature range by effectively preventing NH_3 molecule from non-selective oxidation to generate NO and other undesirable molecules [8–16]. In addition, the fact that such stable Cu^{2+}-2Z species are ought to be beneficial for inhibiting the accumulation of CuOx clusters during hydrothermal aging [14,16,34], evidently contributes to higher catalytic activity of Cu-CHA-D than Cu-CHA-T after hydrothermal aging at 750 °C. Therefore, more Cu^{2+}-2Z species in CHA-D with more paired Al atoms in 6MR should be responsible for the exceeding high-temperature performance and hydrothermal stability in NH_3-SCR reaction. In a word, what can be conclude in this work is that catalytic performance is essentially affected by structure properties in the zeolite framework, especially with respect to Al sites, which rely on the rational choice of organic templates in the synthesis strategy. Such correlation mechanism can be derived from detailed molecular level understanding on crystallization pathways designed by organic templates.

Table 1
Distributions of different types of Al atoms in CHA-T and CHA-D samples as measured by DR UV–vis spectroscopy and ICP tests after being exchanged with Co^{2+} ions.

Samples	$Al_{isolated}$ (%)	Al_{close} (%)	σ type (%)	τ type (%)	ω type (%)
CHA-T	52.3	47.7	1.5	58.1	40.4
CHA-D	16.4	83.6	14.4	38.1	47.5

4. Conclusions

In a summary, effects of the organic templates for the synthesis of SSZ-13 zeolites on the location of Al sites in the framework as well as the catalytic properties have been investigated through using two kinds of organic templates $TMAda^+$ and $DMCHA^+$ cations. 2D ^1H DQ-SQ NMR results demonstrate that the formation of microporous structures could favor the different conformers of the organic templates, and the organic-inorganic interactions between the organic cations and the inorganic framework play an important structure direction role in the assembly of zeolites. The strong electrostatic interactions from $TMAda^+$ cation support the preferential formation of 8MRs in CHA-T, while the coordination effects from $DMCHA^+$ cation induce the preferential formation of D6R units in CHA-D, as evidenced by UV Raman spectra. DR UV–vis spectra with Co(II) as probing cation suggest that the location of Al sites in CHA-D is spatially closer than CHA-T resulted from the different crystallization pathways by the favorable shape and size of organic templates. The fact that CHA-D samples possess more paired Al atoms than CHA-T qualitatively correlates with the superior catalytic activity over CHA-D in high temperature for NH_3-SCR reaction, compared with CHA-T. Our findings have systematically established the relationship of zeolites among synthesis-structure-activity, and

highlighted the importance of crystallization pathways effected by rational choice of organic templates under molecular level investigation. Those detailed understandings will contribute to the development of various zeolite catalysts with controlled Al sites in the pores for improving the catalytic performance for standard NH_3-SCR reaction. This strategy might be applied to prepare other highly efficient zeolite catalysts in the future.

Credit author statement

Juan Zhang designed this project, and prepared, characterized, tested the catalyst, as well as writing the manuscript. **Zhaochi Feng** helped the UV Raman spectroscopic experiments. **Yulong Shan**, **Jinpeng Du**, and **Hong He** performed the catalytic performances of standard NH_3-SCR and NH_3-oxidation reaction. **Shichao Han** executed the ICP tests. **Ling Zhang** and **Chi Lei** helped in data analysis. **Sen Wang** and **Weibin Fan** carried out the DR UV–vis spectroscopic investigation for Al sites. **Xiaolong Liu** provided the ^{1}H MAS NMR and 2D ^{1}H DQ-SQ NMR testing experiments. **Feng-Shou Xiao** and **Xiangju Meng** supervised and provided instructive discussions, wrote the manuscript, and revised on this manuscript.

Declaration of Competing Interest

The authors declare that they have no known competing financial interests or personal relationships that could have appeared to influence the work reported in this paper.

Acknowledgements

This work is supported by National Key Research and Development Program of China (2017YFB0702800), National Natural Science Foundation of China (21720102001, 91634201, and 2152780065), and Strategic Priority Research Program of Chinese Academy of Sciences (XDB17000000).

Appendix A. Supplementary data

Supplementary material related to this article can be found, in the online version, at doi:https://doi.org/10.1016/j.apcatb.2020.119193.

References

[1] A. Corma, Chem. Rev. 97 (1997) 2373–2420.
[2] T. Yokoi, H. Mochizuki, S. Namba, J.N. Kondo, T. Tatsumi, J. Phys. Chem. C 119 (2015) 15303–15315.
[3] Z.Z. Zhao, R. Yu, R.R. Zhao, C. Shi, H. Gies, F.-S. Xiao, D.D. Vos, T. Yokoi, X.H. Bao, U. Kolb, M. Feyen, R. McGuire, S. Maurer, A. Moini, U. Müller, W.P. Zhang, Appl. Catal. B-Environ. 217 (2017) 421–428.
[4] O.H. Han, C.S. Kim, S.B. Hong, Angew. Chem. Int. Ed. 41 (2002) 469–472.
[5] A. Janda, A.T. Bell, J. Am. Chem. Soc. 135 (2013) 19193–19207.
[6] T. Zhang, F. Qiu, J.H. Li, Appl. Catal. B-Environ. 195 (2016) 48–58.
[7] C. Paolucci, A.A. Parekh, J.R. Di Iorio, H. Li, J.D.A. Caballero, A.J. Shih, T. Anggara, W.N. Delgass, J.T. Miller, F.H. Ribeiro, R. Gounder, W.F. Schneider, J. Am. Chem. Soc. 138 (2016) 6028–6048.
[8] K.P. Xie, J.W. Woo, D. Bernin, A. Kumar, K. Kamasamudram, Appl. Catal. B-Environ. 24 (2019) 205–216.
[9] C. Paolucci, I. Khurana, A.A. Parekh, S. Li, A.J. Shih, H. Li, J.R. Di Iorio, J.D.A. Caballero, A. Yezerets, J.T. Miller, Science 357 (2017) 898–903.
[10] R. Daya, S.Y. Joshi, J.Y. Luo, R.K. Dadi, N.W. Currier, A. Yezerets, Appl. Catal. B-Environ. 263 (2020) 118368–118379.
[11] S.A. Bates, A.A. Verma, C. Paolucci, A.A. Parekh, T. Anggara, A. Yezerets, W.F. Schneider, J.T. Miller, W.N. Delgass, F.H. Ribeiro, J. Catal. 312 (2014) 87–97.
[12] J.H. Kwak, H. Zhu, J.H. Lee, C.H.F. Peden, J. Szanyi, Chem. Commun. 48 (2012) 4758–4760.
[13] A.M. Beale, I.L. Gonzalez, W.A. Slawinksi, D.S. Wragg, Chem. Commun. 52 (2016) 6170–6173.
[14] J. Song, Y.L. Wang, E.D. Walter, N.M. Washton, D.H. Mei, L. Kovarik, M.H. Engelhard, S. Prodinger, Y. Wang, C.H.F. Peden, F. Gao, ACS Catal. 7 (2017) 8214–8227.
[15] J.R. Di Iorio, C.T. Nimlos, R. Gounder, ACS Catal. 7 (2017) 6663–6674.
[16] Y.L. Shan, W.P. Shan, X.Y. Shi, J.P. Du, Y. Bo, H. He, Appl. Catal. B-Environ. 264 (2020) 118511–118520.
[17] U. Deka, I.L. Gonzalez, B.M. Weckhuysen, A.M. Beale, ACS Catal. 3 (2013) 413–427.
[18] T.Y. Liang, J.L. Chen, Z.F. Qin, J.F. Li, P.F. Wang, S. Wang, G.F. Wang, M. Dong, W.B. Fan, J.G. Wang, ACS Catal. 6 (2016) 7311–7325.
[19] V. Pashkova, S. Sklenak, P. Klein, M. Urbanova, J. Dědeček, Chem. Eur. J. 22 (2016) 3937–3941.
[20] J.R. Di Iorio, R. Gounder, Chem. Mater. 28 (2016) 2236–2247.
[21] T. Biligetu, Y. Wang, T. Nishitoba, R. Otomo, S. Park, H. Mochizuki, J.N. Kondo, T. Tatsumi, T. Yokoi, J. Catal. 353 (2017) 1–10.
[22] Y.R. Leshkov, M. Moliner, M.E. Davis, J. Phys. Chem. C 115 (2011) 1096–1102.
[23] A.B. Pinar, L.G. Hortigüela, L.B. McCusker, J.P. Pariente, Chem. Mater. 25 (2013) 3654–3667.
[24] K. Muraoka, W. Chaikittisilp, Y. Yanaba, T. Yoshikawa, T. Okubo, Angew. Chem. Int. Ed. 57 (2018) 3742–3746.
[25] A.B. Pinar, R. Verel, J.P. Pariente, J.A. Van Bokhoven, Microporous Mesoporous Mater. 193 (2014) 111–114.
[26] T. Yokoi, H. Mochizuki, S. Namba, J.N. Kondo, T. Tatsumi, J. Phys. Chem. C 119 (2015) 15303–15315.
[27] J. Devos, M.L. Bols, D. Plessers, C.V. Goethem, J.W. Seo, S.J. Hwang, B.F. Sels, M. Dusselier, Chem. Mater. 32 (2020) 273–285.
[28] N. Sheng, Y.Y. Chu, S.H. Xin, Q. Wang, X.F. Yi, Z.C. Feng, X.J. Meng, L.X. Long, F. Deng, F.-S. Xiao, J. Am. Chem. Soc. 138 (2016) 6171–6176.
[29] P.K. Dutta, J. Twu, J. Phys. Chem. 95 (1991) 2498–2501.
[30] X.L. Liu, Q. Luo, J. Phys. Chem. C 121 (2017) 13211–13217.
[31] F.T. Fan, Z.C. Feng, K.J. Sun, M.L. Guo, Q. Guo, Y. Song, W.X. Li, C. Li, Angew. Chem. Int. Ed. 48 (2009) 8743–8874.
[32] J. Dědeček, E. Tabor, S. Sklenak, ChemSusChem 12 (2019) 556–576.
[33] M.M. Treacy, J.B. Higgins, R.V. Ballmoos, Zeolites 5 (1996) 327–328.
[34] Y.L. Shan, J.P. Du, W.P. Shan, X.Y. Shi, H. He, Appl. Catal. B-Environ. 266 (2020) 118655–118667.
[35] H. Lee, I. Song, S.W. Jeon, D.H. Kim, React. Chem. Eng. 4 (2019) 1059–1066.
[36] F. Gao, Y.l. Wang, N.M. Wsahton, M. Kollár, J. Szanyi, C.H.F. Peden, ACS Catal. 5 (2015) 6780–6791.
[37] F.D. Liu, K. Asakura, H. He, W.P. Shan, X.Y. Shi, C.B. Zhang, Appl. Catal. B-Environ. 103 (2011) 369–377.
[38] S.L. Burkett, M.E. Davis, J. Phys. Chem. 98 (1994) 4647–4653.
[39] M.G. O'Brien, A.M. Beale, C.R.A. Catlow, B.M. Weckhuysen, J. Am. Chem. Soc. 128 (2006) 11744–11745.
[40] T. Ikuno, W. Chaikittisilp, Z.D. Liu, T. Iida, Y. Yanaba, T. Yoshikawa, S. Kohara, T. Wakihara, T. Okubo, J. Am. Chem. Soc. 137 (2015) 14533–14544.
[41] Y. Yu, G. Xiong, C. Li, F.-S. Xiao, Microporous Mesoporous Mater. 46 (2001) 23–34.
[42] S.H. Ahn, H. Lee, S.B. Hong, Chem. Mater. 29 (2017) 5583–5590.
[43] W. Mozgawa, W. Jastrzebski, M. Handke, J. Mol. Struct. 744–747 (2005) 663–670.
[44] J. Zhang, Y.Y. Chu, X.L. Liu, X. Hao, X.J. Meng, Z.C. Feng, F.S. Xiao, Chin. J. Catal. 40 (2019) 1854–1859.
[45] J. Dědeček, V. Balgova, V. Pashkova, P. Klein, B. Wichterlova, Chem. Mater. 24 (2012) 3231–3239.
[46] K. Mlekodaj, J. Dědeček, V. Pashkova, E. Tabor, P. Klein, M. Urbanova, R. Karcz, P. Sazama, S.R. Whittleton, H.M. Thomas, A.V. Fishchuk, S. Sklenak, J. Phys. Chem. C 123 (2019) 7968–7987.
[47] W.J. Mortier, J.J. Pluth, J.V. Smith, Mater. Res. Bull. 12 (1977) 97–102.
[48] W.J. Mortier, J.J. Pluth, J.V. Smith, Mater. Res. Bull. 12 (1977) 241–249.
[49] M.L. Bols, S.D. Hallaert, B.E.R. Snyder, J. Devos, D. Plessers, H.M. Rhoda, M. Dusselier, R.A. Schoonheydt, K. Pierloot, E.I. Solomon, B.F. Sels, J. Am. Chem. Soc. 140 (2018) 12021–12032.